A&A 560, A88 (2013)
DOI: 10.1051/0004-6361/201321834

Astronomy & Astrophysics

Dust-to-metal ratios in damped Lyman-α absorbers

Fresh clues to the origins of dust and optical extinction towards γ-ray bursts

A. De Cia[1,2], C. Ledoux[3], S. Savaglio[4], P. Schady[4], and P. M. Vreeswijk[1]

[1] Department of Particle Physics and Astrophysics, Faculty of Physics, Weizmann Institute of Science, 76100 Rehovot, Israel
e-mail: annalisa.de-cia@weizmann.ac.il
[2] Centre for Astrophysics and Cosmology, Science Institute, University of Iceland, Dunhagi 5, 107 Reykjavik, Iceland
[3] European Southern Observatory, Alonso de Córdova 3107, 19001 Casilla, Santiago 19, Chile
[4] Max-Planck Institut für Extraterrestrische Physik, Giessenbachstraße 1, 85748 Garching, Germany

Received 5 May 2013 / Accepted 18 September 2013

ABSTRACT

Motivated by the anomalous dust-to-metal ratios derived in the literature for γ-ray burst (GRB) damped Lyman-α absorbers (DLAs), we measure these ratios using the dust-depletion pattern observed in UV/optical afterglow spectra associated with the interstellar medium (ISM) at the GRB host-galaxy redshifts. Our sample consists of 20 GRB absorbers and a comparison sample of 72 DLAs toward quasars (QSOs) with redshift $1.2 < z < 4.0$ and down to $Z = 0.002\,Z_\odot$ metallicities. The dust-to-metal ratio in QSO- and GRB-DLAs increases both with metallicity and metal column density, spanning ~10–110% of the Galactic value and pointing to a nonuniversal dust-to-metal ratio. The low values of dust-to-metal ratio suggest that low-metallicity systems have lower dust fractions than typical spiral galaxies and, perhaps, that the dust in these systems is produced inefficiently, i.e. by grain growth in the low-metallicity regime with negligible contribution from supernovae (SNe) and asymptotic giant branch (AGB) stars. On the other hand, some GRB- and QSO-DLAs show high dust-to-metal ratio values out to $z \sim 4$, requiring rapid dust production, such as in SN ejecta, but also in AGB winds and via grain growth for the highest metallicity systems. GRB-DLAs overall follow the dust-to-metal-ratio properties of QSO-DLAs, GRBs probing larger column and volume densities. For comparison, the dust-to-metal ratio that we derive for the SMC and LMC are ~82–100% and ~98% of the Galactic value, respectively. The literature dust-to-metal ratio of the low-metallicity galaxy I Zw 18 (<37%) is consistent with the distribution that we find. The dust extinction A_V increases steeply with the column density of iron in dust, $N(\mathrm{Fe})_{\mathrm{dust}}$, calculated from relative metal abundances, confirming that dust extinction is mostly occurring in the host galaxy ISM. Most GRB-DLAs display $\log N(\mathrm{Fe})_{\mathrm{dust}} > 14.7$, above which several QSO-DLAs reveal molecular hydrogen, making GRB-DLAs promising candidates for molecular detection and study.

Key words. gamma-ray burst: general – ISM: abundances – dust, extinction – quasars: absorption lines

1. Introduction

The interplay between the production/recycling of metals and the formation/evolution of cosmic dust is strongly connected with star formation (e.g., Gall et al. 2011a; Cortese et al. 2012) and plays a fundamental role in the chemical enrichment of the interstellar medium (ISM). One way of estimating the dust content along the line of sight is through the optical dust extinction A_V (e.g., Pei 1992). The low-ionization gas content is typically traced by the neutral hydrogen $N(\mathrm{H\,I})$, while a possible probe of the metals is the soft X-ray absorption $N(\mathrm{H})_\mathrm{X}$ (e.g. Morrison & McCammon 1983; Wilms et al. 2000). $A_V/N(\mathrm{H\,I})$ can then be used to infer the dust-to-gas ratio. However, this ratio does not provide a natural way to quantify the amount of dust in a galaxy's ISM as it does not include the metals in the gas. On the other hand, the dust-to-metal ratio, i.e. the fraction of metals in dust, represents the ability of a system to produce or destroy dust grains. Besides, it can be derived regardless of the H I constraint, which is often not available (see Sect. 2). We refer to $\mathcal{DTM}$ to indicate the dust-to-metal ratios normalized by the Galactic value.

The dust-to-metal ratio in the Galaxy is $A_V/N(\mathrm{H})_\mathrm{X}[\mathrm{Gal}] \sim 5.6 \times 10^{-22}$ mag cm^2 (Predehl & Schmitt 1995; Güver & Özel 2009; Watson 2011, the latter two providing a 20% lower value), in agreement with the measurements based on UV absorption lines (Bohlin et al. 1978). The Small Magellanic Cloud (SMC) and Large Magellanic Cloud (LMC) have $A_V/N(\mathrm{H})_\mathrm{X}[\mathrm{SMC}]$[1] $\sim 2.8 \times 10^{-22}$ mag cm^2 and $A_V/N(\mathrm{H})_\mathrm{X}[\mathrm{LMC}]$[1] $\sim 5.3 \times 10^{-22}$ mag cm^2, corresponding to ~50% and ~95% of the Galactic value, respectively. Such measurements are typically difficult to carry out for distant galaxies. Dai & Kochanek (2009) studied the ratio in gravitationally lensed galaxies at $z < 1$ by comparing the extinction curve and the X-ray absorption in the spectra of multiply-imaged quasars (QSOs) in the background. They find the dust-to-metal ratio to range from ~10% to a few times the Galactic value, but with large uncertainties. Brinchmann et al. (2013) recently derived dust-to-metal ratios increasing with metallicity for super-solar metallicity galaxies based on observed CO absorption and the theoretical expectations of Charlot & Longhetti (2001).

Long-duration (>2 s) γ-ray bursts (GRBs) can offer the unique possibility of directly probing the gas, dust, and metal

[1] This value is derived from the observed $E(B-V)/N(\mathrm{H})$ from Martin et al. (1989) and Draine (2003) and converting it to $N(\mathrm{H})_\mathrm{X}/A_V$ assuming $R_V = 2.9, 3.2$ (Pei 1992; Draine 2003) and a mean [Zn/H] = −0.64, −0.55 for the SMC and LMC respectively (Welty et al. 1997, 1999).

content in their star-forming host galaxy, out to very high redshifts. Their afterglows are often bright enough to allow absorption-line spectroscopy that can reveal the H I gas and metal column densities in the ISM (e.g., Savaglio et al. 2003; Vreeswijk et al. 2004; Berger et al. 2006; Prochaska et al. 2007; Ledoux et al. 2009; Fynbo et al. 2009). In addition, the well-understood power-law continuum (e.g., Sari et al. 1998; Piran 1999) facilitates the determination of the intrinsic A_V and $N(\mathrm{H})_\mathrm{X}$ (e.g., Campana et al. 2006; Krühler et al. 2011; Zafar et al. 2011a; Schady et al. 2012). The latter is measured for most *Swift* bursts (Evans et al. 2009) and A_V can be studied out to $z > 6$ (Schady et al. 2010; Zafar et al. 2011b). In contrast, the same measurements are more difficult to make towards QSOs, due to the presence of broad emission lines contaminating a large fraction of their optical/ultraviolet continuum. The samples of GRB absorbers that are typically followed up for spectroscopic studies are biased against the most dusty systems that have been dimmed by large A_V's or faint GRBs. A fraction of GRB host galaxies is massive and dusty (Krühler et al. 2011; Hunt et al. 2011; Rossi et al. 2012; Perley et al. 2013). Nevertheless, the current (biased) samples are still representative of the majority of the GRB host population, i.e., low-mass, low-metallicity and actively star-forming galaxies (e.g. Savaglio et al. 2009).

Zafar et al. (2011a) and Schady et al. (2010) investigated the dust-to-metal ratios for a large sample of distant GRB-selected galaxies using $A_V/N(\mathrm{H})_\mathrm{X}$. They found $A_V/N(\mathrm{H})_\mathrm{X}$ in GRBs that were up to two orders of magnitude lower than what had been observed in the Local Group, confirming the results of Galama & Wijers (2001). This implies that either damped Lyman-α absorbers (DLAs) associated with GRB host galaxies have different dust-to-metal ratios or that A_V and $N(\mathrm{H})_\mathrm{X}$ probe different regions along the line of sight. While the dust is expected to lie in the cold low-ionization medium, the X-ray absorption traces the metals regardless of their ionization state. The evidence of ionization induced by the GRB on the surrounding medium, in the immediate environment of the GRB for most bursts and out to hundreds of pc for absorbing systems with low $N(\mathrm{H\,I})$ (De Cia et al. 2012; Vreeswijk et al. 2013), confirms that indeed the line of sight analysis can be affected by ionization and dust destruction. Thus, the $A_V/N(\mathrm{H})_\mathrm{X}$ may not provide the best estimate of the dust-to-metal ratio for GRB host galaxies. Recent estimates based on line of sight A_V, $N(\mathrm{H\,I})$ and the metallicity suggest that the dust-to-metal ratios in GRB and QSO absorbers are roughly constant around the Galactic value (Zafar & Watson 2013).

An alternative approach to calculate the extragalactic dust-to-metal ratios is based on the dust-depletion pattern revealed by UV/optical absorption-line spectroscopy. Using such methods, the dust-to-metal ratios in QSO-DLAs and a few GRB-DLAs were found to be consistent with or slightly lower than the Galactic value (Vladilo 1998; Savaglio 2001; Savaglio et al. 2003; Savaglio & Fall 2004; Vladilo 2004). One of the advantages of using optical absorption lines rather than dust extinction to determine the dust content is that the absorption lines refer to a particular redshift and thus they are not integrated along the whole line of sight. This is particularly crucial for low-metallicity systems with an intrinsically low dust content and for high-z targets, whose lines of sight likely cross intervening galaxies, each contributing to A_V.

In this paper, we develop a new dust-depletion-based method to derive the dust-to-metal ratios, cross-checked with the Savaglio (2001, S01 hereafter) method, and apply it to a sample of 20 GRB absorbers (observed at medium to high spectral resolution) and 72 QSO-DLAs (all with high-resolution spectroscopy). This approach solely relies on the observation of optical/UV low-ionization absorption lines associated with DLAs and therefore there is little or no ambiguity on the location or ionization state of the absorbing gas/dust: we purely focus on the bulk of the ISM in the host galaxies, which is mostly far-away from the GRB (e.g., hundreds of parsecs from the burst Vreeswijk et al. 2007, 2011) and therefore not affected by ionization due to the GRB or the progenitor.

The paper is organized as follows. Our sample is defined in Sect. 2 and the methods of our analysis are explained in Sect. 3. The results are presented in Sect. 4 and discussed in Sect. 5. Finally, we summarize our conclusions in Sect. 6. Throughout the paper we adopt ions cm^{-2} as the linear unit of column densities N. We refer to relative abundances of two chemical elements X and Y defined as $[X/Y] \equiv \log \frac{N(X)}{N(Y)} - \log \frac{N(X)_\odot}{N(Y)_\odot}$. For the reference solar abundances appearing in the second term of this formula, we use the values of Asplund et al. (2009) and follow the recommendations of Lodders et al. (2009) by adopting the photospheric estimates for the more volatile elements, the meteoritic estimates for the less refractory elements, or the average between them (see details in De Cia et al. 2012). The quoted errors and limits correspond to 1σ and 3σ significance levels, respectively, unless otherwise stated.

2. The GRB-DLA sample

We select all GRB absorbers with a constrained estimate of the column density of Fe II, and of at least one ion among Zn II and Si II, from the largest sample to date of GRB absorber column densities collected by Schady et al. (2011). The resulting sample is composed of 20 GRB absorbers in the redshift range $1.2 < z < 4.0$ and spans a wide range of metallicities (from $Z \sim 2\,Z_\odot$ down to $Z \sim 0.005\,Z_\odot$), listed in Table 1. Most absorbers have an H I estimate from Lyman-α, all but one with $\log N(\mathrm{H\,I}) > 20.3$ and therefore classified as DLAs (Wolfe et al. 1986). One exception is GRB 090323 with $\log N(\mathrm{H\,I}) = 19.6$ for one of the two absorbing systems that composes its line profile. The column density estimates of the GRB sample are derived from absorption-line spectroscopy, using curve-of-growth analysis for the spectra with low or medium resolution (see details in Schady et al. 2011, and references therein) and Voigt profile fitting for a handful of high-resolution spectra (Vreeswijk et al. 2007; Ledoux et al. 2009).

3. Revisiting the dust-to-metal ratio for GRB-DLAs: the Savaglio (2001) recipe and a new method

It is possible to estimate the dust-to-metal ratio from the depletion in dust of different elements, observed with optical/UV absorption-line spectroscopy, in particular from Fe II and Zn II lines. While H I is fundamental to deriving the overall metallicity, it is not necessary to derive this ratio. Fe II and Zn II are two elements that have a similar nucleosynthetic history, but very different depletion properties. Fe is typically heavily depleted onto dust grains, while Zn is only mildly depleted (e.g., Savage & Sembach 1996; Ledoux et al. 2002) and is therefore a metallicity indicator. Thus, we use [Fe/Zn] as a dust indicator, where the reliability of iron as a tracer of the bulk of the dust is explained in Appendix A. Si and S, also quite abundant in the ISM, can be useful dust-depletion indicators as well, but should be treated with caution, especially in the case of S (e.g., Jenkins 2009), as explained in Appendix B. Besides, the depletion of Si is typically not significant enough to make [S/Si] a solid dust indicator at low metallicity.

Table 1. Dust-to-metal ratios normalized by the Galactic value ($\mathcal{DTM}$) derived with the method described in this paper and Savaglio's (2001, S01).

GRB	z	A_V (mag)	log N(H I)	[X/H][a]	[X/Fe]	X	$\mathcal{DTM}$ (new)	[X/H]$_{tot}$[b]	log[c] N(Fe)$_{dust}$	$\mathcal{DTM}$ (S01)	log $Z/Z_\odot$[d]	J[e]
990123	1.60	<0.25			2.01 ± 0.18	Zn	1.12 ± 0.00		$17.05^{+0.45}_{-0.30}$	$1.11^{+0.16}_{-0.11}$		all
000926	2.04	0.38 ± 0.05	21.30 ± 0.20	-0.11 ± 0.21	1.06 ± 0.21	Zn	1.06 ± 0.04	$+0.03^{+0.34}_{-0.37}$	$16.77^{+0.27}_{-0.19}$	$1.00^{+0.20}_{-0.20}$		D
010222	1.48	$0.24^{+0.08}_{-0.09}$			1.30 ± 0.17	Zn	1.09 ± 0.02		$16.78^{+0.33}_{-0.23}$	$1.22^{+0.02}_{-0.02}$		H
020813	1.25				0.90 ± 0.07	Zn	1.02 ± 0.03		$16.45^{+0.25}_{-0.18}$	$0.98^{+0.20}_{-0.01}$		D
030226$_{s1}$[f]	1.99	0.05 ± 0.01	20.50 ± 0.30	-0.94 ± 0.30	0.17 ± 0.04	Si	0.47 ± 0.09	$-0.87^{+0.34}_{-0.35}$	$14.72^{+0.19}_{-0.15}$	$0.58^{+0.09}_{-0.20}$	$-0.78^{+0.08}_{-0.07}$	DW
030226$_{s2}$[f]	1.96	0.05 ± 0.01	20.50 ± 0.30	-1.04 ± 0.30	0.45 ± 0.03	Si	0.86 ± 0.06	$-0.86^{+0.38}_{-0.39}$	$14.99^{+0.24}_{-0.15}$	$0.89^{+0.04}_{-0.20}$	$-0.77^{+0.05}_{-0.05}$	DW
030323	3.37		21.90 ± 0.07	-1.26 ± 0.27	0.18 ± 0.27	Si	0.49 ± 0.43	$-1.19^{+0.25}_{-0.22}$	<16.46	$0.66^{+0.61}_{-0.49}$	$-1.08^{+0.45}_{-0.39}$	HDW
050401	2.90	0.45 ± 0.03	22.60 ± 0.30	-0.93 ± 0.42	1.14 ± 0.36	Zn	1.07 ± 0.05	$-0.78^{+0.64}_{-0.73}$	$17.27^{+0.53}_{-0.45}$	$1.19^{+0.04}_{-0.04}$		H
050730	3.97	<0.17	22.10 ± 0.10	-2.14 ± 0.10	0.12 ± 0.05	Si	0.36 ± 0.12	$-2.09^{+0.12}_{-0.13}$	$14.98^{+0.27}_{-0.27}$	$0.66^{+0.29}_{-0.33}$	$-1.76^{+0.63}_{-0.32}$	HWC
050820A	2.62	0.27 ± 0.04	21.05 ± 0.10	-0.72 ± 0.10	0.98 ± 0.12	Zn	1.04 ± 0.03	$-0.59^{+0.21}_{-0.23}$	$15.89^{+0.23}_{-0.15}$	$1.00^{+0.18}_{-0.13}$		HWC
050922C	2.20	$0.14^{+0.08}_{-0.07}$	21.55 ± 0.10	-2.09 ± 0.12	0.35 ± 0.27	Si	0.76 ± 0.24	$-1.95^{+0.12}_{-0.16}$	$14.89^{+0.31}_{-0.58}$	$0.81^{+0.22}_{-0.20}$	$-1.85^{+0.14}_{-0.13}$	DW
051111	1.55	$0.39^{+0.11}_{-0.10}$			0.99 ± 0.04	Zn	1.04 ± 0.02		$16.41^{+0.25}_{-0.17}$	$1.00^{+0.15}_{-0.10}$		all
060418	1.49	$0.13^{+0.01}_{-0.02}$			0.71 ± 0.03	Zn	0.95 ± 0.04		$15.95^{+0.17}_{-0.11}$	$0.88^{+0.20}_{-0.02}$		D
070802	2.45	$1.23^{+0.18}_{-0.16}$	21.50 ± 0.20	-0.16 ± 0.24	0.37 ± 0.18	Zn	0.70 ± 0.19	$-0.11^{+0.34}_{-0.38}$	$16.65^{+0.25}_{-0.22}$	$0.61^{+0.09}_{-0.09}$		C
071031	2.69	<0.11	22.15 ± 0.05	-1.76 ± 0.05	0.03 ± 0.03	Zn	0.08 ± 0.07	$-1.76^{+0.07}_{-0.07}$	$14.74^{+0.09}_{-1.26}$	$0.07^{+0.07}_{-0.05}$		all
080330	1.51	<0.19			0.93 ± 0.11	Zn	1.03 ± 0.04		$15.71^{+0.26}_{-0.19}$	$0.99^{+0.17}_{-0.12}$		all
080413A	2.43	<0.88	21.85 ± 0.15	-1.63 ± 0.16	0.12 ± 0.07	Zn	0.30 ± 0.14	$-1.61^{+0.21}_{-0.22}$	$15.13^{+0.14}_{-0.36}$	$0.27^{+0.13}_{-0.10}$		HWC
090323$_{s1}$[f]	3.58	0.10 ± 0.04	19.62 ± 0.33	$+0.33 \pm 0.35$	0.51 ± 0.14	Si	0.91 ± 0.10	$+0.53^{+0.46}_{-0.50}$	$15.52^{+0.35}_{-0.26}$	$0.94^{+0.20}_{-0.20}$	$0.60^{+0.16}_{-0.16}$	D
090323$_{s2}$[f]	3.57	0.10 ± 0.04	20.72 ± 0.09	$+0.22 \pm 0.10$	1.41 ± 0.06	Zn	1.10 ± 0.01	$+0.40^{+0.28}_{-0.30}$	$16.58^{+0.32}_{-0.22}$	$1.23^{+0.01}_{-0.01}$		H
090926A	2.11	<0.15	21.73 ± 0.07	-2.27 ± 0.27	0.57 ± 0.30	Si	0.94 ± 0.16	$-2.05^{+0.25}_{-0.34}$	$15.07^{+0.50}_{-0.40}$	$1.01^{+0.24}_{-0.20}$	$-1.94^{+0.38}_{-0.35}$	HDW

Notes. Uncertainties refer to a 1σ confidence level, while 3σ limits are reported for unconstrained measurements. [(a)] Observed abundance of the element X relative to solar. [(b)] Abundances corrected for dust depletion. When available, [Zn/H]$_{tot}$ is considered to be the metallicity of the gas. [(c)] Column density of iron in dust-phase (see text). [(d)] Metallicity as fitted with the S01 method (Eq. (1)), when H is unconstrained and Zn constrained. [(e)] Galactic environments fitted with the S01 method: halo (H), disk + halo (D), warm disk (W) and cool disk (C), as characterized by Savage & Sembach (1996). When more than one environment is possible, $\mathcal{DTM}$(S01) and log $Z/Z_\odot$ are averaged among the allowed values. [(f)] Different absorbing systems toward the same GRB are reported separately.

References. All column densities, z and A_V are taken from the compilation by Schady et al. (2011).

3.1. The S01 method

We derive the $\mathcal{DTM}$ (referred to as k/k_J[2] in S01) from the depletion pattern, i.e., from the observed abundance of different elements, as compared to the depletion pattern observed in different Galactic environments: halo (H), disk+halo (DH), warm disk (WD), and cool disk (CD), as listed in Savage & Sembach (1996). Following the recommendation of Jenkins (2009), we update the mean depletion values listed in Table 6 of Savage & Sembach (1996) slightly by adding −0.03, −0.04, and −0.01 to the values for Fe, Si, and S respectively, here and throughout the paper. The abundances with respect to H or Zn observed in GRB-DLAs are fitted simultaneously assuming that the Galactic depletion patterns, providing a best-fit $\mathcal{DTM}$ and environment type. When both H I and Zn II are constrained, we treat the metallicity [Zn/H] as an input. Instead, when H I is available but not Zn, we fit for the metallicity $Z/Z_\odot$ as well. In practice, we iterate among the different Galactic environments J and sum over different metals X to minimize the total difference between the observed abundances and the reference abundances

$$[X/\mathrm{H}]_{\mathrm{ref}} = \log(1 + \mathcal{DTM} \cdot (10^{dXj} - 1)) + \log(Z/Z_\odot), \quad (1)$$

where dXj is the depletion of a metal X for a given environment J. More details can be found in S01 and Savaglio et al. (2003). We exclude upper and lower limits on the abundances from the fit. We include measurements for at least two metals X among Zn, Si, and Fe. The results of the depletion pattern fit for each absorber are shown in the Appendix (Figs. C.1 and C.2, for the case with and without H I constraints respectively). Sulphur is not included in the fit because it has shown controversial depletion patterns in different Galactic environments (Jenkins 2009), as described in Appendix B. The inclusion of silicon also must be taken with caution as the intrinsic abundance of Si with respect to Fe and Zn may not depend entirely on dust, but instead it could be boosted by α-element enhancements in star-forming galaxies. This leads to a possible degeneracy between the best-fit $\mathcal{DTM}$, metallicity, and Galactic environments. We explore this possibility of an intrinsically lower Si by calculating the $\mathcal{DTM}$s for slightly lower Si column densities than observed (log N(Si) − 0.2 dex). The effect of such change is mostly accounted for by i) setting an upper error on the $\mathcal{DTM}$ of at least 0.2 for best-fit WD and DH environments, when Si is included in the fit and ii) setting a lower error on the $\mathcal{DTM}$ of at least 0.2 when Zn is not constrained.

3.2. A new method for deriving the dust-to-metal ratio for DLAs

Here we derive the absolute dust-to-metal ratio (dtm) based on fundamental definitions and applying depletion corrections to the observed relative abundance of Fe with respect to Zn. The basic idea starts from the definition of the observed [Fe/Zn], where the observed gas-phase column density of an element X

[2] d/d_J in Savaglio et al. (2003) and Savaglio & Fall (2004).

is $N(X)_{\rm obs} = N(X)_{\rm tot} - N(X)_{\rm dust}$. If we assume that Zn is not depleted into dust and if Fe and Zn share the same nucleosynthesis (total of gas- and dust-phase $[{\rm Fe/Zn}]_{\rm tot} = 0$), then a simplified version of the dust-to-metal ratio follows $\mathrm{dtm}_{\rm simplified} = 1 - 10^{[{\rm Fe/Zn}]_{\rm obs}}$.

To include the possible depletion of Zn[3], we assume that the depletion of an element in dust is proportional to a depletion strength factor F_*. This factor represents the overall strength of the dust depletion and it is unique to each line of sight, similar to what has been found for the Galaxy (Jenkins 2009, e.g., their Fig. 7). In the Galaxy, systems with little dust have $F_{*,\rm G} = 0$ and almost no depletion of Zn, but the dustier systems $F_{*,\rm G} = 1$ and even Zn is significantly depleted. We note that the F_* scale for DLAs does not necessarily have to be the same as in the Galaxy because DLAs on average have lower metallicity and presumably lower dust contents. These linear depletion sequences reflect the tendency of each element to condensate in dust grains, i.e., they are related to the condensation temperature of each element (Field 1974; Jenkins 2009). Given that the slopes (dFe, dZn, dSi, et cetera) of these linear relations are specific to each element, the relative composition of the dust grains changes depending on the amount of dust in the environment.

While the slopes and offsets of these linear depletion sequences have been well measured for the Galaxy (Jenkins 2009), in principle, we do not know how these relations change for lower-metallicity environments such as most DLAs. The observed offsets in the Galaxy are interpreted as pre-existing dust grains that cause some level of depletion even for the less dusty systems (Jenkins 2009). For the GRB and QSO sample of absorbers, we assume no offsets in the depletion sequences ($\delta_X = 0$ at $F_* = 0$), meaning that for DLAs we assume no pre-existing grains. This is expected given the relatively high redshift and the low metallicity of QSO- and GRB-DLAs, only a handful of which are above [Zn/H] ~ -0.3 in our DLA sample. Moreover, the evidence that most metal-poor DLAs (with assigned $F_* = 0$) show [Zn/Fe] ~ 0 (Noterdaeme et al. 2008; Molaro et al. 2000), i.e., no depletion, unambiguously reveals no offset in the DLA depletion sequences[4].

In this way, the depletion of Zn and Fe can be described as

$$\delta_{\rm Zn} = [{\rm Zn/H}]_{\rm obs} - [{\rm Zn/H}]_{\rm intrinsic} = d{\rm Zn} \cdot F_* \quad (2a)$$

$$\delta_{\rm Fe} = [{\rm Fe/H}]_{\rm obs} - [{\rm Fe/H}]_{\rm intrinsic} = d{\rm Fe} \cdot F_*, \quad (2b)$$

where $[{\rm Zn/H}]_{\rm intrinsic}$ and $[{\rm Fe/H}]_{\rm intrinsic}$ are the total abundances in the gas and dust phases, and when $F_* = 1$, $\delta_{\rm Zn} = d{\rm Zn}$. Since the observed (depleted) abundances are associated with the gas-phase metals, the fraction of an element X in gas f_X is

$$f_X = 10^{\delta_X}. \quad (3)$$

Figure 1 visualizes these relations and the quantities we derive below. Note that we do not assume solar abundances or fixed grain compositions, rather we rely on the observed relative abundances $[{\rm Fe/Zn}]_{\rm obs}$ as a function of the depletion strength. Since

$$F_* = (\delta_{\rm Fe} - \delta_{\rm Zn})/(d{\rm Fe} - d{\rm Zn}) = [{\rm Fe/Zn}]_{\rm obs}/(d{\rm Fe} - d{\rm Zn}), \quad (4)$$

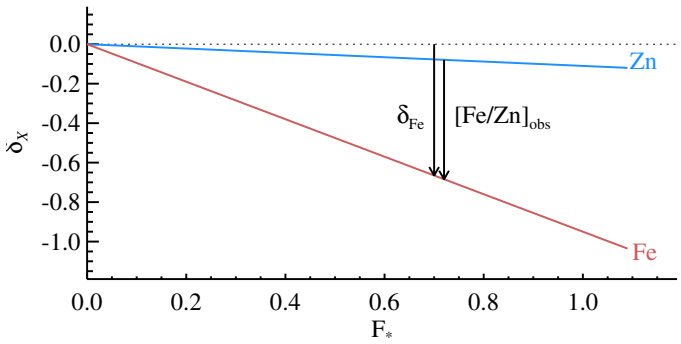

Fig. 1. A scheme displaying two linear depletion sequences of Zn and Fe with the depletion strength factor F_*. Although F_* is not known for a given line of sight, it can be traced by the observed [Zn/Fe] ratio.

the dust to metals ratio dtm is then defined as

$$\mathrm{dtm} = \frac{N({\rm Fe})_{\rm dust}}{N({\rm Fe})_{\rm tot}} = 1 - 10^{\delta_{\rm Fe}} = 1 - 10^{[{\rm Fe/Zn}]_{\rm obs}\, d{\rm Fe}/(d{\rm Fe} - d{\rm Zn})}. \quad (5)$$

This definition of dtm assumes only two linear dust depletion sequences for Fe and Zn respectively, and that Zn and Fe have the same nucleosynthetic history ($[{\rm Fe/Zn}]_{\rm tot} = 0$), so any deviation of [Fe/Zn] from solar is due to dust depletion.

The slopes of the depletion sequences correspond to the expected level of depletion in the most dusty ($F_* = 1$) DLA systems. We assume dFe $= -0.95$, dSi $= -0.26$ and dZn $= -0.11$, i.e., the average depletion along disk+halo lines of sight[5] of Fe and Si (Savage & Sembach 1996) and Zn (Roth & Blades 1995). This translates to ~90% of Fe, ~45% of Si, and ~20% of Zn having been depleted into dust for the dustiest DLAs. The assumption of steeper slopes, such as the Galactic dFe $= -1.28$, dSi $= -1.14$, and dZn $= -0.61$ (Jenkins 2009), would overestimate the dust-corrected metallicities (see Sect. 5.1 for a discussion on the dependence of our results on the assumed slopes). Thus, we limit our analysis to the slope values mentioned above and include an uncertainty of 0.1 on the slopes to allow for some freedom.

Finally, we normalize the dtm values with respect to the Galactic value

$$\mathcal{DTM} = \mathrm{dtm}/\mathrm{dtm(G)}, \quad (6)$$

where dtm(G) = 0.89 (see the Appendix C for its derivation).

Another useful quantity that can be derived from the above formalism is the column density of iron in dust, $N({\rm Fe})_{\rm dust}$ (Col. 9 of Table 1), which provides an estimate of the dust content in the ISM, independently from A_V. Given that

$$N({\rm Fe})_{\rm tot} = N({\rm Zn})_{\rm tot} \times \left(\frac{N({\rm Fe})}{N({\rm Zn})}\right)_\odot \quad (7)$$

and

$$N({\rm Zn})_{\rm tot} = \frac{N({\rm Zn})_{\rm obs}}{f_{\rm Zn}} = \frac{N({\rm Zn})_{\rm obs}}{10^{[{\rm Zn/Fe}]_{\rm obs}\, d{\rm Zn}/(d{\rm Zn} - d{\rm Fe})}}, \quad (8)$$

the dust-phase column density of iron is

$$\begin{aligned} N({\rm Fe})_{\rm dust} &= N({\rm Fe})_{\rm tot} \times \mathrm{dtm} = \\ &= 10^{[{\rm Fe/Zn}]_{\rm obs}} \times (10^{[{\rm Fe/Zn}]_{\rm obs}\, d{\rm Fe}/(d{\rm Zn} - d{\rm Fe})} - 1) \\ &\quad \times N({\rm Zn})_{\rm obs} \times \left(\frac{N({\rm Fe})}{N({\rm Zn})}\right)_\odot \\ &= N({\rm Fe})_{\rm obs} \times (10^{[{\rm Fe/Zn}]_{\rm obs}\, d{\rm Fe}/(d{\rm Zn} - d{\rm Fe})} - 1). \end{aligned} \quad (9)$$

[3] Some level of Zn depletion should be taken into account, given that GRBs are likely to reside in star-forming regions, some of them with a potentially significant dust content (e.g., Perley et al. 2013).

[4] In the Galactic line-of-sight sample of Jenkins (2009), the least dusty systems were not entirely dust-free, thereby leading to the observed Galactic offsets.

[5] Disk + halo lines of sight: HD 18100, HD 167756.

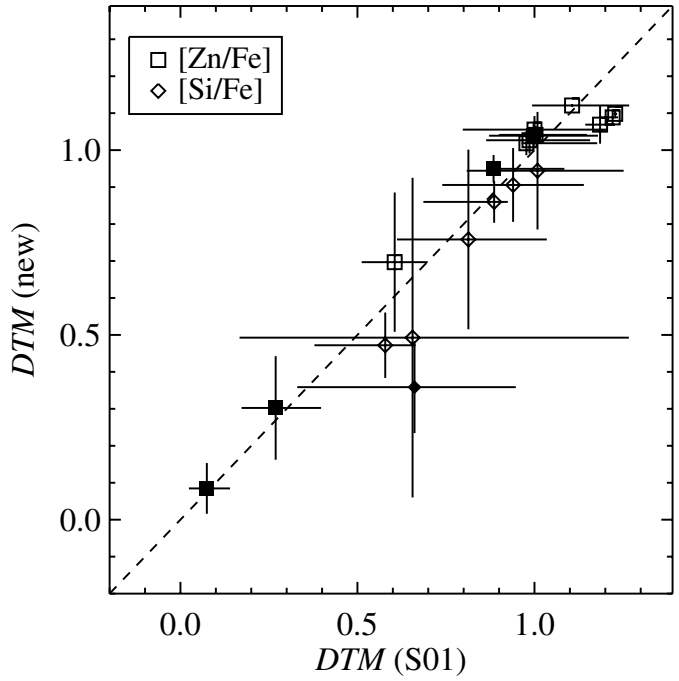

Fig. 2. Comparison between the $\mathcal{DTM}$ derived with the new and the S01 methods. The symbols indicate which metal was used as a reference to calculate the [X/Fe] ratio, where [Zn/Fe] is the most reliable ratio because it is less sensitive to intrinsic abundance changes. The filled symbols highlight the DLAs with high-resolution spectroscopy, which typically have more robust constraints. The vicinity to the equality (dashed) line shows the agreement between the two estimates.

Table 2. Spearman's rank correlation coefficients ρ and significance.

x^a	y^a	Fig.	DLA	ρ^b	P^c	σ
$\mathcal{DTM}$(S01)	$\mathcal{DTM}$	2	GRB	0.94	<0.001	6.15
$[\mathrm{Zn/H}]_{\mathrm{TOT}}$	$\mathcal{DTM}$	3	QSO	0.660	<0.001	3.8
			GRB	0.667	0.050	1.96
$\log N(\mathrm{Zn\,II})_{\mathrm{TOT}}$	$\mathcal{DTM}$	3	QSO	0.464	0.013	2.48
			GRB	0.632	0.020	2.32
$[X/\mathrm{H}]_{\mathrm{TOT}}{}^d$	$\mathcal{DTM}$	4	QSO	0.564	<0.001	4.9
			GRB	0.604	0.022	2.29
$\log N(\mathrm{Zn\,II})_{\mathrm{TOT,Eq}}{}^e$	$\mathcal{DTM}$	4	QSO	0.265	0.062	1.86
			GRB	0.682	<0.001	3.31
z	$\mathcal{DTM}$	5	QSO	−0.052	0.671	0.43
			GRB	−0.338	0.144	1.46
$N(\mathrm{Fe})_{\mathrm{dust,Zn,Si}}$				0.702	0.011	2.54
$N(\mathrm{Fe})_{\mathrm{dust,Zn}}$				0.357	0.385	0.88
$N(\mathrm{Fe})_{\mathrm{dust,Si}}$	A_V	6	GRB	0.305	0.392	0.86
$N(\mathrm{Fe})_{\mathrm{dust,Zn}}{}^f$				0.357	0.431	0.79
$N(\mathrm{Fe})_{\mathrm{dust,Si}}{}^f$				0.798	0.010	2.58
$N(\mathrm{H\,I})$	$\mathcal{DTM}$	C.3	QSO	−0.123	0.318	1.00
			GRB	−0.513	0.021	2.31

Notes. [(a)] x- and y-axis sample populations for the correlation test. [(b)] $-1 \leq \rho \leq +1$, where $\rho = +1(-1)$ for perfect monotonic increasing (decreasing) correlations. [(c)] Null-hypothesis probability, where the number of σ indicates the level of significance of the correlation. [(d)] X is either Zn or Si. [(e)] Zn or equivalent Zn column density derived from Si, see Fig. 4. [(f)] Excluding the outlier GRB 070802.

4. Results

4.1. Comparison among $\mathcal{DTM}$ methods

The $\mathcal{DTM}$ derived with the new and the S01 methods for our GRB-DLA sample are listed in Table 1 and plotted against each other in Fig. 2, for comparison. The two methods show a general good agreement and thus we consider them as equivalent (as also confirmed by a Spearman rank test[6]). The results of this test are listed in Table 2. There is a possible small deviation toward higher $\mathcal{DTM}$(S01) above 1, for three GRB absorbers, namely GBR 010222, GRB 050401, and GRB 090323, absorbing system 2. We discuss whether such deviation could affect our results in Sect. 5. The overall reliability of both methods is strengthened by the agreement of the two different $\mathcal{DTM}$ derivations because they are independent from each other.

In addition to the $\mathcal{DTM}$ ratios, the S01 method also provides estimates of the metallicity in case the H column density is constrained but Zn is unconstrained, and the environment type (halo, warm disk, cool disk, disk + halo, as characterized by Savage & Sembach 1996). These are listed in the last two columns of Table 1. Note that when Si is constrained but Zn is unconstrained, the metallicity fitted from the depletion pattern is always higher than the observed [Si/H], as expected from the depletion of Si. Among the best-fit environments, a cool disk is somewhat disfavored for GRB absorbers, although a single best-fit environment could not be constrained for about half of our sample.

In the early stages of the current analysis we also derived the dust-to-metal ratio using the prescription of Vladilo (1998), but we do not include those results because of the assumption of a constant grain composition (fixed fraction of each element in dust). Nevertheless, it is worth reporting that those dust-to-metal ratios are consistent with the results presented here.

4.2. Comparison with QSO-DLAs

To compare the GRB- and QSO-DLA populations, we calculate the $\mathcal{DTM}$ for a sample of 72 QSO-DLAs from Noterdaeme et al. (2008), all of which have been observed with the high-resolution Very Large Telescope (VLT) Ultraviolet and Visual Echelle Spectrograph (UVES, Dekker et al. 2000). We choose to compute the $\mathcal{DTM}$ of QSO-DLAs with our new method because it is easily derived from the [X/Fe] reported in Noterdaeme et al. (2008). The overall sample of GRB- and QSO-DLAs spans a wide range of metallicities, from $Z \sim 2\,Z_\odot$ down to $Z \sim 0.002\,Z_\odot$. The average observed [Zn/Fe] in the QSO and GRB samples are 0.4 and 0.9, respectively, with a standard deviation of 0.2 and 0.5. This suggests that GRB environments are more dusty overall than QSO-DLAs. Indeed, only less than ∼10% of QSO-DLAs show significant reddening due to dust (Khare et al. 2012).

Figure 3 shows the distribution of $\mathcal{DTM}$s, derived with the new method, in GRB-DLAs (black) and QSO-DLAs (grey) as a function of metallicity (left panel) and the Zn column density (right panel) corrected for dust depletion using Eq. (8). The depletion corrections are typically very small, up to ∼0.3 dex. In Fig. 4, we also include those targets that have measurements of the Si column density but lack measurements of the Zn column density. The $\mathcal{DTM}$ that has been estimated from Zn should be

[6] This indicates only how tight a monotonic correlation between two quantities is, but they do not necessarily need to be linear.

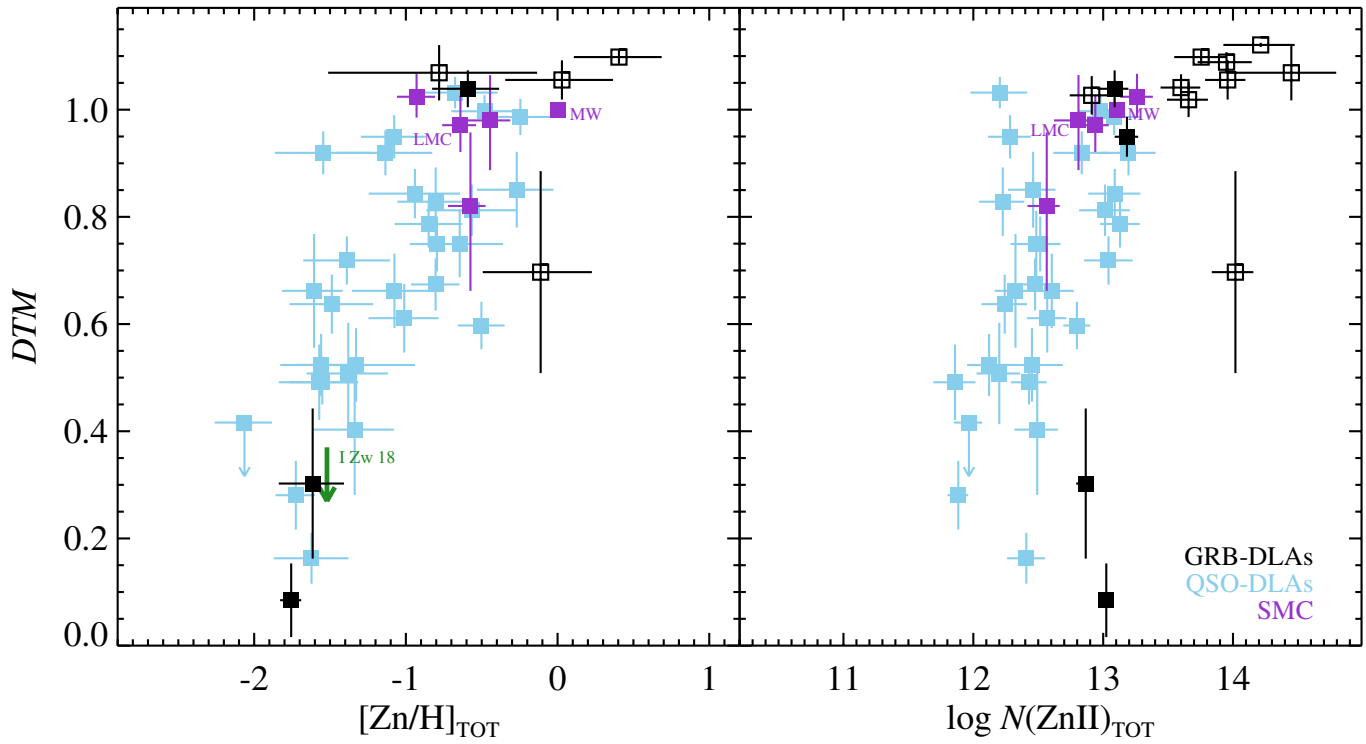

Fig. 3. *Left*: distribution of the $\mathcal{DTM}$ with dust-corrected $[\mathrm{Zn/H}]_{\mathrm{TOT}}$ (the intrinsic metallicity), for the GRB-DLAs (black) in our sample and the UVES QSO-DLAs (gray) sample of Noterdaeme et al. (2008). The MW, SMC (three lines of sight) and LMC $\mathcal{DTM}$ values are displayed for comparison, where the latter two are two representative values derived from the observed [Zn/Fe] along two lines of sight (see text for details). Filled symbols highlight the measurements drawn from high-resolution spectroscopy. The thick green arrow shows the literature value (derived from the $M_{\mathrm{dust}}/M_{\mathrm{H}}$ measured by Herrera-Camus et al. 2012) for the nearby blue compact dwarf galaxy I Zw 18. *Right*: the distribution of the $\mathcal{DTM}$ with the total column density of Zn II, corrected for dust depletion.

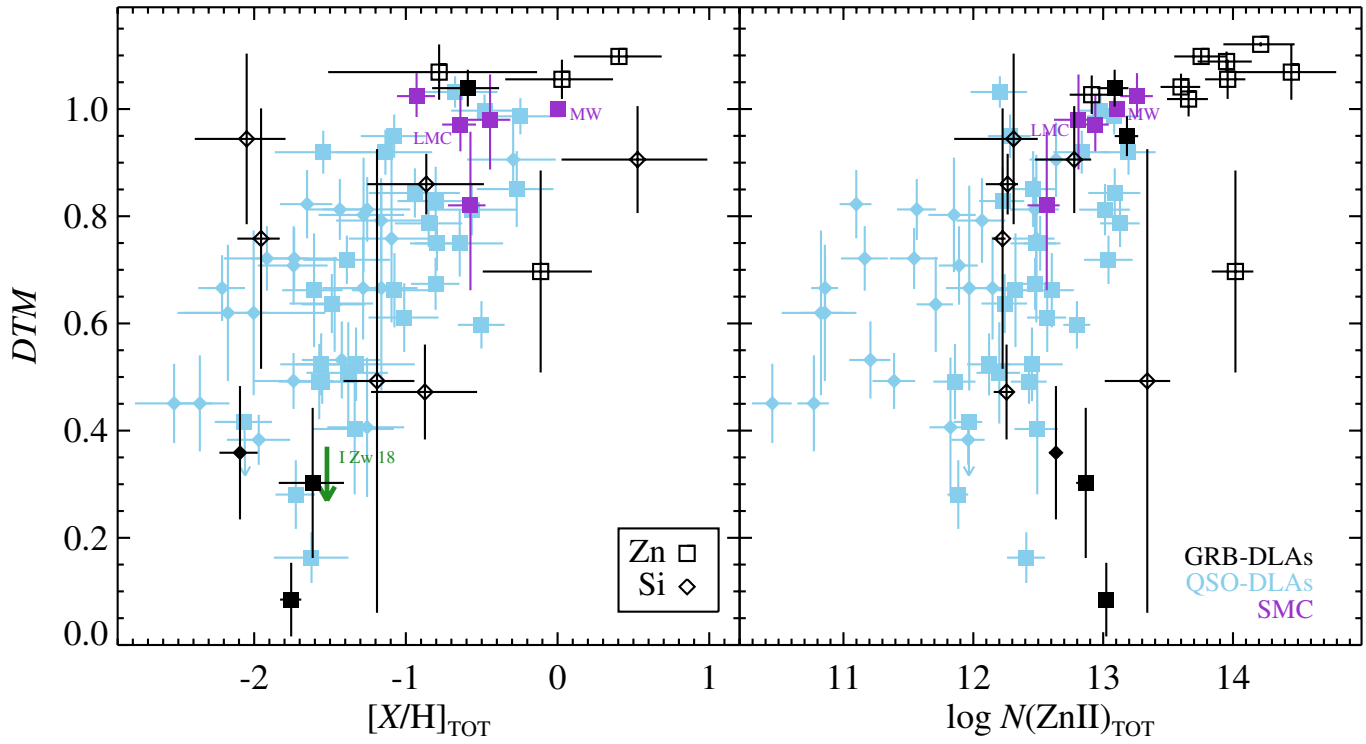

Fig. 4. Same as Fig. 3, but including the $\mathcal{DTM}$ values that have been estimated from Si and thus are less reliable. When Zn is not directly constrained, we display the equivalent Zn II column density derived from the Si II column density, assuming solar relative abundances. The symbols indicate which metals are used in [*X*/Fe] to derive the $\mathcal{DTM}$.

considered more reliable because the [Zn/Fe] is less affected by intrinsic changes of relative abundances than [Si/Fe].

4.3. Comparison with the Magellanic Clouds

We calculate the $\mathcal{DTM}$ values for two lines of sight through the SMC and the LMC, using the Zn and Fe column densities derived from the absorption lines observed in the literature. For the SMC, we consider the absorption in spectra of the background star Sk 108 (Welty et al. 1997)[7], Sk 155, and Sk 78 (Welty et al. 2001). For the LMC, we use the absorption toward supernova SN 1987A (Welty et al. 1999)[8]. While the choice of a few specific line of sight per system may not represent the overall properties of the whole cloud, we note that typically only one line of sight can be observed toward both GRB and QSO as well. The derived $\mathcal{DTM}$ are ~82–100% and ~98% of the Galactic value for the SMC and the LMC, respectively, as displayed in Figs. 3 and 4. Given the similar [Zn/H] and $\log N$(Zn) of the SMC and LMC absorbers, it is interesting to note that the LMC has a higher [Zn/Fe], $\mathcal{DTM}$, and ultimately a larger amount of dust with respect to SMC, although these differences are not 3σ significant.

5. Discussion

5.1. Strengths, caveats, and implications of our $\mathcal{DTM}$ method

The estimates of the dust-to-metal ratio presented in this paper rely purely on the metal absorption lines observed in the optical/UV afterglow spectra. These are selected at the GRB redshift, typically arising in the ISM of the host galaxy, hundreds of parsecs from the burst (e.g., Vreeswijk et al. 2007, 2011).

The main assumption of our $\mathcal{DTM}$ method is the existence of linear depletion sequences in DLAs similar to what has been observed in the Galaxy (Jenkins 2009). These sequences depend on the condensation temperature of each chemical element and naturally explain different dust-grain compositions in different environments. While the slopes of the Galactic depletion sequences are well studied (Jenkins 2009), the corresponding slopes in DLAs are unknown. Here we discuss how much our results depend on the assumption of these slopes.

At the low metallicity end, i.e., in the least dusty DLAs, the low depletions are not very sensitive to changes in slopes (see Fig. 1), while the zero offsets of the linear sequences are fully justified by the observation of [Zn/Fe] ~ 0 in low-metallicity systems (see also Sect. 3.2). For the most dusty DLA systems, the dependence on the slopes of the depletion sequences are more significant. In comparison with the Galactic values however, we find that the possible range of slopes is limited. The slopes of the depletion sequences for DLAs must be shallower than in the Galaxy to provide reasonable dust-corrected metallicities in the DLAs. Indeed, using the Galactic values of the depletion-sequences slopes generally gives a small increase of $\mathcal{DTM}$ (up to ~0.15), but implies excessive metallicities. In the most extreme cases, the Galactic slopes lead to dust-corrected metallicities of up to $Z \sim 7\,Z_\odot$ and $Z \sim 120\,Z_\odot$ for GRB 000926, and GRB 090926A, which are individual absorbing systems with [Zn/Fe]- and [Si/Fe]- based $\mathcal{DTM}$ respectively. These values are too large to be realistic. These numbers are even more extreme for dustier absorbers such as GRB 090323, where the Galactic slopes lead to dust-corrected $Z \sim 30\,Z_\odot$ and $Z \sim 10^4\,Z_\odot$ for the two separate absorbing systems. These results are not justifiable, regardless of the degeneracy of the H I content between the two absorbing systems. On the other hand, the slopes that we assumed for DLAs provide dust-corrected metallicities $Z \sim 1.1\,Z_\odot$, $Z \sim 0.01\,Z_\odot$, $Z \sim 3.4\,Z_\odot$, and $Z \sim 2.5\,Z_\odot$ for the systems mentioned above, respectively. Thus, the depletion levels of Si, Fe, and Zn are likely more moderate in DLAs than in the Galaxy. The $\mathcal{DTM}$ values given in Table 1 are probably reliable within the errors, despite the uncertainties in the slopes of the depletion sequences in DLAs.

The depletion of Fe and Zn of the most dusty DLAs (with depletion factor $F_* \sim 1$ and above) are similar to what has been observed in the least dusty lines of sight in the Galaxy (with Galactic depletion factor $F_{*,\mathrm{G}} \sim 0$, Jenkins 2009), such as disk + halo lines of sight studied by Savage & Sembach (1996). One intriguing possibility is that the depletion factor could evolve continuously from the least depleted dust-free DLAs to the most dusty Galactic lines of sight, where the depletion sequences would start at $F_* = 0$ with no offset and shallow slopes and gradually evolve into the observed Galactic depletion sequences.

5.2. The $\mathcal{DTM}$ distribution

The $\mathcal{DTM}$ distribution of the GRB-DLAs in our sample increases with metallicity and spans ~10%–110% of the Galactic value. In addition, the observed trend points to low dust fractions for low-metallicity systems, which is inconsistent with a constant Galactic $\mathcal{DTM}$ at any metallicity, as recently suggested (e.g., Zafar & Watson 2013). Given these results, it is clear that $A_V/N(\mathrm{H})_\mathrm{X}$ should not be considered a reliable estimate of the dust-to-metal ratios in GRB-DLAs.

The comparison between GRB- and QSO-DLAs in Fig. 3 reveals a continuous distribution of the $\mathcal{DTM}$ between the two populations, indicating an overall similarity of their ISMs. The mean $\mathcal{DTM}$ for GRBs and QSOs are 0.8 and 0.6 respectively, with a standard deviation of 0.3 and 0.2. Given that GRB lines of sight preferentially cross through inner (and more dusty) regions of their star-forming galaxies, while QSO lines of sight typically intercept the haloes of intervening galaxies (e.g., Prochaska et al. 2007; Fynbo et al. 2009), GRBs probe the $\mathcal{DTM}$ distribution up to one order of magnitude larger column densities than QSO lines of sight. In the Galaxy, the average volume density of the gas is tightly correlated with the depletion factor ($F_{*,\mathrm{G}} = 0.772 + 0461 \times \log\langle n(\mathrm{H})\rangle$, Jenkins 2009). For DLAs, we derive the average volume density from the observed the depletion factor F_* (Eq. (4)), using the relation observed in the Galaxy. While the actual values of $\langle n(\mathrm{H})\rangle$ that we find for DLAs may be unreliable because the relation might evolve with metallicity and be different for DLAs, the comparison between the densities in QSO- and GRB-DLAs are meaningful. While QSO-DLAs have $0.001 < \langle n(\mathrm{H})\rangle < 10$ cm^{-3}, several GRB-DLAs exceed 10 cm^{-3}, confirming that GRBs are typically located in denser regions than QSO absorbers.

The $\mathcal{DTM}$ increases with metallicity (Figs. 3 and 4, left panels). Despite the large scatter, the increasing trend is clear up to $[X/\mathrm{H}] \sim -1$. Above this metallicity the distribution may be consistent with a roughly constant dust-to-metal ratio for DLAs, as

[7] We refer to the mean observed [Zn/Fe] = 0.50 ± 12 and [Zn/H] = $-0.64^{+0.13}_{-0.17}$ associated with the SMC, consistent with [Zn/Fe] = 0.66 ± 20 measured by Sofia et al. (2006) for the same line of sight.

[8] We refer to the mean [Zn/Fe] = $0.78^{+0.12}_{-0.16}$ and [Zn/H]= −0.55 ± 0.08, averaged among the velocity components associated with the LMC.

found by Zafar & Watson (2013) based on A_V. At lower metallicities we find low $\mathcal{DTM}$ values in both QSO- and GRB-DLAs, which are not constant and not consistent with the Local Group, pointing to a nonuniversal dust-to-metal ratio.

The discrepancy between our results and the A_V-derived $\mathcal{DTM}$ (Zafar & Watson 2013, although only one single datapoint is constrained at very low metallicities) might arise from an overestimate of the intrinsic dust content when estimated from the line-of-sight A_V of the lower-metallicity and less dusty systems. For these low-dust systems the additional extinction due to foreground absorbers along the whole line of sight contribute significantly to the A_V. Indeed, the observed foreground $E(B-V)$ toward QSOs typically ranges between ~0.001 and ~0.1 (Ménard et al. 2008), i.e., $0.003 \lesssim A_V \lesssim 0.3$, so this additional source of dust extinction can be significant when compared to the intrinsically low A_V of very low-metallicity systems. On the other hand, our dust-depletion analysis does not suffer from the contribution of intervening systems and therefore provides reliable estimates of the dust content of low-metallicity systems.

In Figs. 3 and 4, we include a literature estimate of the $\mathcal{DTM}$ of the blue compact dwarf galaxy I Zw 18, one of the lowest-metallicity systems known in the local universe ([O/H] = −1.52, $M_{\rm dust}/M_{\rm H} < 8.1 \times 10^{-5}$; Herrera-Camus et al. 2012), where we consider the dust-to-metal mass ratio $M_{\rm dust}/M_{\rm met} = 10^{\log(M_{\rm dust}/M_{\rm H}) - [{\rm O/H}]}$ and normalize it by the Galactic value $(M_{\rm dust}/M_{\rm H})_{\rm Gal} = 0.0073$ (Draine et al. 2007). The $\mathcal{DTM} < 0.37$ of I Zw 18 is consistent with the trend that we find for GRB- and QSO-DLAs, supporting the idea that low metallicity systems have lower dust fractions than typical spiral galaxies.

The $\mathcal{DTM}$ distribution increases with the metal column density as well (represented by the Zn or the equivalent Zn column density, right panel of Fig. 3) and flattens out above $\log N({\rm Zn}) \sim 13$. One issue that needs to be clarified is whether this flattening is physical or is artificially introduced by our analysis. As noted in Sect. 4, our method might slightly underestimate three $\mathcal{DTM}$ values (see Fig. 2), all of which have $\log N({\rm Zn}) > 13$. However, given the magnitude of the effect, these three points are unlikely to prove crucial. The observed flattening of the $\mathcal{DTM}$ at higher metal column densities might suggest that the availability of metals in the ISM can drive dust formation/growth up to some stable level where metals are largely accessible, as is the case for the Galaxy. Dust destruction due to GRBs might also play a role in limiting the amount of dust (e.g., Waxman & Draine 2000; Draine & Hao 2002).

The significance of the correlations described above is confirmed by a Spearman rank test, as listed in Table 2, indicating that $\mathcal{DTM}$ is most tightly correlated with [Zn/H]. There is a much weaker correlation between the $\mathcal{DTM}$ distribution and the H I column density, as shown in Fig. C.3 in the Appendix. This confirms that the dust traces the metals rather than the total gas content.

While the $\mathcal{DTM}$ values in QSOs are uniformly distributed, we cannot exclude the presence of two populations of GRB hosts divided by their $\mathcal{DTM}$ properties, i.e., a standard one following the trends that have been observed for QSO-DLAs and a second group of GRB-DLAs with a lower $\mathcal{DTM}$. This is most notable in the $\mathcal{DTM}$ distribution against the metal column density, although the gap is less evident when also including $\mathcal{DTM}$ estimates derived from Si. It is difficult to assess whether this separation is a real effect, given the small number statistics. If true, these low-$\mathcal{DTM}$ GRB-DLAs (mostly GRB 071031 and GRB 080413A) may correspond to systems having a smaller amount of dust for their metal content, possibly due to sputtering or sublimation of dust grains in actively star-forming regions (Tielens et al. 1994; Waxman & Draine 2000). Further observations are clearly needed to investigate this issue.

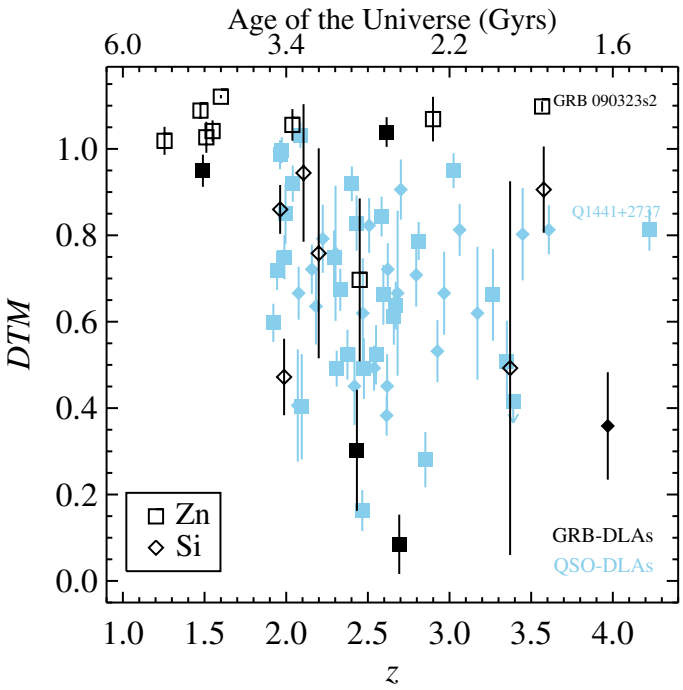

Fig. 5. $\mathcal{DTM}$ evolution with redshift. The symbols are the same as in Fig. 4.

We do not observe any trend of the $\mathcal{DTM}$ with the mass, star-formation rate, or specific star-formation rate of the host galaxies, although the sample for which all these estimates are available is limited to a handful of objects (Vreeswijk et al. 2004; Chen et al. 2009; Savaglio et al. 2009; Krühler et al. 2011; Savaglio et al. 2012).

5.3. On the origin of dust in DLAs

We further explore the evolution of the $\mathcal{DTM}$ with redshift, as displayed in Fig. 5. Combined with the metallicity information, this provides some further clues on the dust production in DLAs.

5.3.1. At low redshift

All the estimated $\mathcal{DTM}$ values for GRB-DLAs below $z \sim 1.7$ (6 out of 20) are large and similar to the Galactic value. While the metallicity of these systems has not been measured from absorption lines because Ly-α is not redshifted into the observable window, the Zn II column densities of these absorbers are all above $\log N({\rm Zn\,II}) \gtrsim 13$ (with the exception of GRB 080330 with $\log N({\rm Zn\,II}) \sim 12.8$ D'Elia et al. 2009). Low-z GRB absorbers follow the $\mathcal{DTM}$ distribution with the metal column density discussed above and it is reasonable to expect that they follow the $\mathcal{DTM}$ distribution with metallicity as well. If so, this would indicate that at redshift below $z \lesssim 1.7$ most GRBs occur in galaxies with metallicities $Z \gtrsim 0.1\ Z_\odot$, possibly because the mean metallicity of star-forming galaxies has increased with cosmic evolution. However, this result should be viewed with caution because the number of observations at low redshift is limited.

5.3.2. At high redshift

While the $\mathcal{DTM}$ distribution shows a large scatter above $z \gtrsim 1.7$, we confirm the evidence for some high-$\mathcal{DTM}$ galaxies, such as GRB 090323 at $z = 3.6$ (Savaglio et al. 2012) or QSO-DLA Q 1441+2737 at $z = 4.2$ (Ledoux et al. 2006), to lie at high redshift. The presence of dusty systems at these redshifts suggests that a rapid dust-production mechanism may be required for the dust to have formed well within a Gyr. One such fast mechanism is the condensation of dust grains in cooled SN ejecta (e.g., Matsuura et al. 2011), where the contribution of SNe on dust production is dominant at early times (for time scales below ~200 Myr, Gall et al. 2011a). Asymptotic giant branch (AGB) stars start to recycle their metals into the ISM producing silicates grains after ~40 Myr (Di Criscienzo et al. 2013) and carbon-rich dust after a few hundreds Myr of main-sequence evolution (Galliano et al. 2008). However, at low metallicities the contribution of AGB stars to dust production is unlikely to be significant in systems with young stellar populations (see below). The observation of rapidly-produced dust (within 30–170 Myr) in $z \gtrsim 6$ QSOs suggests that SNe dominate the dust production at these redshifts, with a negligible contribution of AGB stars (Gall et al. 2011b). While SNe are the dominant source of dust at early times, AGB stars are thought to start contributing at $z < 8-10$ (Valiante et al. 2011). However, extinction curves of SN-produced dust (showing a kink at 3000 Å) have not been conclusively constrained in $z \sim 6$ quasars (Hjorth et al. 2013) yet.

Grain growth in the ISM is typically considered a slow process for producing dust, but its time scale decreases with increasing metallicity (the growth time scale τ is of the order of ~60 Myr for solar-metallicity systems, Hirashita & Kuo 2011). Thus, dust production via grain growth cannot be excluded for those systems at high redshift with relatively high metallicity, such as GRB 090323, but also down to a few percent solar metallicity. Moreover, ISM shattering can increase the number of small grain and thereby allow grain growth to account for the amounts of dust observed in high-redshift quasars (Kuo & Hirashita 2012). Besides, grain growth is required to explain the dust content observed in high-redshift quasars (Mattsson 2011; Valiante et al. 2011). While the current observation of the $\mathcal{DTM}$ at $z \sim 4$ cannot put stringent limits on the origin of this dust, future observations of $\mathcal{DTM}$ at redshifts above 5 will be crucial to assess the extent of SN contribution at high redshift (Morgan & Edmunds 2003). The method described in this paper can in principle allow the $\mathcal{DTM}$ to be measured up to very high redshift.

5.3.3. At low metallicities

The low $\mathcal{DTM}$ of $Z \lesssim 0.1\ Z_\odot$ DLAs implies that these systems have a lower fraction of dust with respect to the higher metallicity systems. This could be due to a lower efficiency of dust production and/or a higher efficiency of dust destruction. The efficiency of dust-production from AGB stars is also lower in low-metallicity systems, becoming a negligible source of dust below $Z \sim 0.005\ Z_\odot$ (Di Criscienzo et al. 2013). However, in low-metallicity environments the most massive AGB stars that are short-lived, but not massive enough to explode as SNe ($5\ M_\odot \lesssim M \lesssim 8\ M_\odot$) evolve to become N-rich and O-rich M-stars (Karakas & Lattanzio 2007; Gall et al. 2011c) that are particularly inefficient at forming dust (Ventura et al. 2012). Thus, AGB stars seem to bring a negligible contribution to dust production, when compared to SNe, in low-metallicity systems dominated by young stellar populations. Importantly, SNe dust production is not very sensitive to metallicity changes (Galliano et al. 2008), and thus represents an unlikely source of the $\mathcal{DTM}$ trend with metallicity. On the other hand, below $Z \sim 0.1\ Z_\odot$ grain growth starts to be less efficient and its time scale becomes larger (τ of hundreds of Myr to Gyr, depending on the metallicity and the grain-size distribution; Hirashita & Kuo 2011).

One possible cause of a higher efficiency in dust destruction could be a harder and more intense radiation field produced by enhanced massive-star formation in low-metallicity environments, such as for GRB host galaxies (e.g. Savaglio et al. 2009). However, Gall et al. (2011a) showed that simulated dust masses are higher for initial mass functions with more high-mass stars, meaning that SNe are overall more efficient at producing than destroying dust. An alternative cause of a higher level of dust destruction could be a grain-size distribution skewed toward smaller grains in low-metallicity systems (Sandstrom et al. 2012), since such dust grains are more easily destroyed (e.g., Waxman & Draine 2000). However, this is an unlikely scenario for QSO-DLAs, where sources of dust destruction (shocks or radiation due to SNe or GRBs) are limited. Moreover, an increasing $\mathcal{DTM}$ with increasing metallicity is expected only if there is a net production of dust via grain growth in the ISM over dust destruction (Mattsson et al. 2012)[9]. Thus, the lower fraction of dust in the low-metallicity DLAs could be due to a lower efficiency of dust-production via grain growth, with negligible SN and AGB stars contribution.

5.4. Dust extinction from the host galaxy ISM

Given that the measurement of the dust extinction A_V is integrated along the whole line of sight, it is not trivial to assess whether the intrinsic A_V of the host galaxy is mostly associated with the bulk of the ISM. In principle, there could be a contribution from intervening systems (although they show typically weaker absorption than GRB-DLAs themselves; Vergani et al. 2009) or from a dense and dusty star-forming region associated with the GRB. On the other hand, we use the metal absorption lines to infer the dust column in the host galaxy ISM, specifically the column density of Fe in dust $N(\mathrm{Fe})_{\mathrm{dust}}$ (Eq. (9)). It is insightful to compare A_V and $N(\mathrm{Fe})_{\mathrm{dust}}$ because they are two entirely independent estimates of the dust content: A_V is derived from the continuum shape of the optical/UV afterglow, while $N(\mathrm{Fe})_{\mathrm{dust}}$ is derived from the optical absorption lines produced by metals at the redshift of the host galaxy ISM. We compare these two quantities to investigate whether A_V is produced in the ISM probed by UV absorption lines.

Figure 6 shows that $N(\mathrm{Fe})_{\mathrm{dust}}$ steeply increases with A_V in GRB absorbers, at least up to $A_V \sim 0.5$. The significance of the $N(\mathrm{Fe})_{\mathrm{dust}}$ correlation with A_V is reported in Table 2 for the measurements based on both Si and Zn, and also on the individual elements separately. While the correlation seems more solid when including both Zn and Si (2.5σ significance level), we note that Zn-based measurements alone are not very helpful for the purpose of testing this correlation because of its narrow range of A_V. This arises from the observational difficulty of constraining Zn column densities in low-metallicity systems. The scatter of the correlation is quite large, indicating that in some cases there might be some contribution to the A_V that is not related to the bulk of the host-galaxy ISM, as for the clear outlier

[9] $\mathcal{DTM}$ gradients that are coupled with metallicity gradients are thought to be a signature of the higher efficiency of grain growth over dust destruction (Mattsson et al. 2012).

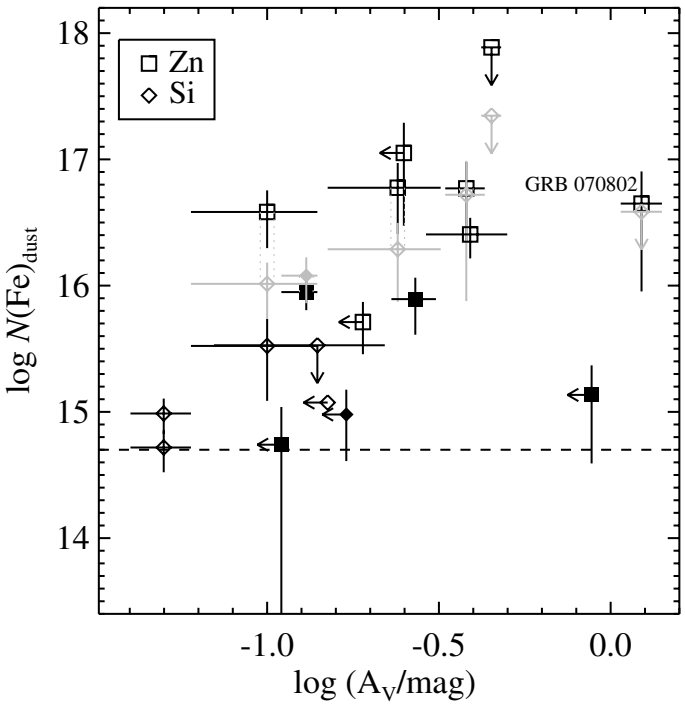

Fig. 6. Optical extinction A_V distribution with the column density of Fe in dust. The dashed line marks the column density above which a significant presence of molecules has been observed in QSO-DLAs (Noterdaeme et al. 2008). When both are available, the measurements derived from Zn and Si are displayed in black and grey, respectively. The symbols are the same as in Fig. 4.

GRB 070802 (see below). Overall, the observed trends strongly support the general idea that A_V is mostly produced in the bulk of the host galaxy ISM. A similar conclusion was also reached by Krühler et al. (2011) and Zafar et al. (2011a).

GRB 070802 stands out from the observed trend with the highest A_V measurement. We note that this is one of the few GRBs where a Galactic-like 2175 Å bump was observed imprinted on the optical afterglow spectrum (Elíasdóttir et al. 2009; Zafar et al. 2012). The high extinction, well above the general trend of Fig. 6, might strengthen the hypothesis that in this case the extinction occurs in two different regions with two different types of grains – one of them not representative of the bulk of the host galaxy – as suggested by Zafar et al. (2012). The observation of the 2175 Å bump and the multi-component nature of A_V makes this line of sight stand out from the rest of the GRB sample. One alternative explanation is that the distribution of $N(\mathrm{Fe})_{\mathrm{dust}}$ flattens out, as if some saturation process prevented iron from further accreting on dust grains above a certain threshold.

In general, one obvious candidate for an additional region to contribute to the A_V, other than the host ISM, is a dense and dusty environment close to the GRB where no low-ionization lines are produced. However, dust-destruction fronts typically move faster and reach greater distances than the ionization fronts produced by GRBs, making the dust destruction more efficient than ionization (Draine & Hao 2002). Thus, it seems unlikely to observe regions with dust but no low-ionization gas. Thus, foreground absorbers are more likely to be the source of additional contribution to the A_V. However, the positive correlation between $N(\mathrm{Fe})_{\mathrm{dust}}$ and A_V confirms that for most lines of sight the main source of extinction is the GRB host galaxy.

5.5. Molecular content

Given the GRB association with massive star-forming regions (e.g., Woosley 1993; Hjorth & Bloom 2012), we expect to observe the signature of molecular clouds in some optical afterglow spectra. In particular, dusty systems may bear the conditions for molecular formation, since dust grains can be efficient catalysts to aid the formation of molecules, such as H_2, on their surfaces (e.g., Pirronello et al. 1997). However, molecular absorption bands are typically weak and notoriously difficult to observe in optical/near-UV spectra of extragalactic sources (e.g., Noterdaeme et al. 2008). In GRB afterglows, CO was detected only once to date in the low-resolution Keck/LRIS spectrum of GRB 080607 (Prochaska et al. 2009), while H_2 has been recently observed in a couple of mid-resolution VLT/X-shooter afterglow spectra (Krühler et al. 2013, Friis et al., in prep.). The dashed line in Fig. 6 shows the column density $\log N(\mathrm{Fe})_{\mathrm{dust}} = 14.7$ above which molecules have been observed in ∼40% of QSO-DLAs (Noterdaeme et al. 2008). Most GRB-DLAs lie above this column density and thus are promising sites to detect molecules.

While the presence of molecules is expected in GRB environments, the hard radiation of the bursts are effective in destroying dust and molecules in molecular clouds (Draine & Hao 2002). However, the currently low detection rate of molecules observed in GRBs may be an observational effect due to the typically low spectral resolution or low S/N of the majority of GRB optical/near-UV spectra. On the other hand, current high-resolution samples might be biased against high metallicity lines of sight (potentially rich in dust and molecules) because only bright afterglows can currently be observed at high spectral resolution (Ledoux et al. 2009). A large sample of mid-resolution (e.g., VLT/X-shooter) spectroscopic observations of GRB-DLAs can potentially include a significant number of those systems with the most favorable conditions for molecular formation (i.e., high H I and relatively high metallicity, Noterdaeme et al. 2008), with sufficient S/N and spectral resolution to constrain the actual molecular content and the extent of dust destruction.

6. Conclusions

We derive the dust-to-metal ratios ($\mathcal{DTM}$) in long-duration GRB- and QSO-DLAs based on the dust-depletion pattern observed from low-ionization metal absorption lines in the optical/UV afterglow spectra. In this way, the dust-to-metal ratio is purely associated with the bulk of the neutral ISM in the GRB- or QSO-DLA, which is not influenced by the GRB, rather than integrated along the total line of sight. As a comparison, we also derive the $\mathcal{DTM}$ of GRB absorbers using a different method based on dust-depletion as well, described in Savaglio (2001), with fully consistent results.

The dust-to-metal ratios in GRB-DLAs span ∼10–110% of the Galactic value and show properties similar to the QSO-DLA distribution, with GRBs extending the study of dust-to-metal ratios out to higher column and volume densities. Above metallicities of $Z \sim 0.1\,Z_{\odot}$, these results are partially consistent with the finding of a universally constant Galactic-like dust-to-metal ratio based on A_V (Zafar & Watson 2013). However, at lower metallicities, down to $Z \sim 0.002\,Z_{\odot}$, we find compelling evidence for low values of $\mathcal{DTM}$ for both GRB- and QSO-DLAs. We argue that our $\mathcal{DTM}$ estimates for low-metallicity DLAs are more reliable than those based on the dust extinction along the line of

sight because low A_V values are more sensitive to the contribution of foreground systems.

The $\mathcal{DTM}$ distribution increases with metallicity and metal column density. A similar trend was recently observed by Brinchmann et al. (2013) for super-solar metallicity nearby galaxies. We observe a flattening of this trend above $\log N(\mathrm{Zn}) \sim 13$, suggesting that the production/destruction of dust with respect to the metals stabilizes for more evolved galaxies. The low dust fraction of low-metallicity systems may be the result of inefficient dust production, e.g., for grain growth in the low-metallicity regime (where the time scale for grain growth becomes too long), with negligible contribution by SNe and AGB stars.

A possibility that needs to be further investigated is the presence of a population of low-$\mathcal{DTM}$ GRB-DLAs having a smaller amount of dust given their metal content, possibly due to destruction of dust grains in actively star-forming regions.

At $z \lesssim 1.7$, all the $\mathcal{DTM}$ estimates for the GRB-DLAs in our sample show high (Galactic-like) values. If confirmed with a larger sample, this may indicate that at lower redshift most GRBs occur in galaxies with $Z \gtrsim 0.1\ Z_\odot$ that are richer in dust with respect to the overall host-galaxies population. This could possibly be due to the overall increase of metallicity with cosmic evolution. The presence of some of these high $\mathcal{DTM}$ galaxies is observed out to $z \sim 4$, indicating that for these systems a fairly rapid ($\lesssim$1 Gyr) production mechanism is required, i.e., in cooled SN ejecta as well as in AGB winds and grain growth in a $Z \sim Z_\odot$ metallicity regime. We find no trends of the $\mathcal{DTM}$ with the host-galaxy mass, star-formation rate, and specific star-formation rate.

The column density of Fe in dust $N(\mathrm{Fe})_{\mathrm{dust}}$ that we derive from the relative abundances observed in the host-galaxy ISM steeply increases with the dust extinction A_V observed toward GRBs, up to at least $A_V \sim 0.5$. This confirms that A_V is mostly produced by the bulk of the ISM neutral gas. At high A_V, we observe one outlier of this trend, GRB 070802, where either an additional contribution for the extinction must be included or the $N(\mathrm{Fe})_{\mathrm{dust}}$ flattens out at high A_V. The majority of GRB-DLAs shows high values of $N(\mathrm{Fe})_{\mathrm{dust}}$ (above $\log N(\mathrm{Fe})_{\mathrm{dust}}$ 14.7, the minimum value for QSO-DLA with molecular detection Noterdaeme et al. 2008), making them promising sites for the detection of molecules.

Acknowledgements. We are most grateful to Edward B. Jenkins and Lars Mattsson for insightful comments on the manuscript. We thank Avishay Gal-Yam, Darach Watson and Tayyaba Zafar for useful discussions. A.D.C. acknowledges support by a Grant of Excellence from the Icelandic Research Fund, the Weizmann Institute of Science Dean of Physics Fellowship, and the Koshland Center for Basic Research.

Appendix A: Iron as a tracer of the bulk of the dust

Relying on the depletion of iron to trace dust one may wonder whether a bias is introduced, affecting systems that have a significant amount of dust but hardly any iron-rich grains. Here we discuss whether this is a significant issue for our analysis. Iron is typically used as a dust tracer because it is highly depleted (60–90% of iron is found in dust grains in the Milky Way, Savage & Sembach 1996; Pinto et al. 2013), while still being easily observable (it is among the most abundant refractory elements in the ISM). After oxygen and carbon, the main dust components in the Milky Way are Mg, Si, and Fe, with about ~30 atoms every 10^6 H atoms (e.g., Kimura et al. 2003; Przybilla et al. 2008). Iron traces a variety of dust compounds, such as silicates (both olivine and pyroxenes contain Fe, besides O, Mg, and Si), oxides (Fe embedded in oxides must contribute to silicate mixtures, Voshchinnikov & Henning 2010) and iron-based dust grains. Iron-poor carbonaceous grains contribute to the dust content as well. However, carbonaceous grains are typically more abundant in Galactic-like environments, where iron-rich grains are also well represented. The typical dust extinction of lower-metallicity environments like SMC is well reproduced with silicate grains without a significant contribution from carbonaceous grains (Pei 1992). This may apply to GRB host galaxies as well, the majority of which show a SMC- or LMC-type extinction curve (Zafar et al. 2011a; Schady et al. 2012).

Ni and Cr could be used as dust tracers instead of Fe as well, but they are not as diffused and as easily observed as iron. [Zn/Fe] typically increases with metallicity as a result of dust depletion of Fe in both QSO- and GRB-DLAs (Ledoux et al. 2002; Savaglio et al. 2003; Wolfe et al. 2005; Dessauges-Zavadsky et al. 2006a; Prochaska et al. 2007; Noterdaeme et al. 2008) and therefore is widely used as a dust indicator. Thus, iron and zinc are the most suitable elements for this analysis and we consider the depletion of iron to be a reliable indicator of the overall amount of dust in GRB host galaxies.

Appendix B: Sulphur

Despite its little depletion onto dust grains, sulphur has been regarded as a "troublesome element" because of its unconventional behavior of the depletion in Galactic environments, often leading to negative depletion strength factor F_* (Jenkins 2009). In general, the observed depletion of S in the Galaxy is sometimes poorly constrained, for instance for halo environments ($-0.2 \lesssim$ [S/H] $\lesssim 0.2$ Savage & Sembach 1996). Besides, S shows an erratic depletion behavior in QSO-DLAs as well where [S/Si] extends down to ~−0.3 (e.g., Dessauges-Zavadsky et al. 2006b), either consistent with solar with a very large scatter, or indicating nonuniform depletion. If not depletion, either nucleosynthesis (S being an α-element) or observational effects are responsible for the observed sulphur behavior. Among the latter, Galactic S II lines are often saturated, while the high-ionization potential of S II (23.3 eV) allows it to survive ionization in H II regions (Jenkins 2009). Given these uncertainties, we disregard S as a reliable tracer of dust (non-) depletion for the current study.

Appendix C: Derivation of the Galactic dust-to-metal ratio

We calculate dtm(G) assuming $[\mathrm{Fe/Zn}]_\mathrm{G} = -0.95$, which is the average value of Galactic disk+halo lines of sight (Savage & Sembach 1996) with the −0.03 dex correction of Jenkins (2009). The slopes of the Galactic depletion sequences are $d\mathrm{Fe}_\mathrm{G} = A_\mathrm{Fe} = -1.285$ and $d\mathrm{Zn}_\mathrm{G} = A_\mathrm{Zn} = -0.610$ (Jenkins 2009, where the depletion formalism is expressed in terms of A, B, and z coefficients). The offsets of the Galactic sequences (i.e., depletion at $F_* = 0$) are $\mathrm{offset}_\mathrm{Fe} = B_\mathrm{Fe} - A_\mathrm{Fe}\, z_\mathrm{Fe} = -0.95$ and $\mathrm{offset}_\mathrm{Zn} \sim 0$, so then

$$\delta_{\mathrm{Zn,G}} = d\mathrm{Zn}_\mathrm{G} \times F_* \tag{C.1a}$$

$$\delta_{\mathrm{Fe,G}} = d\mathrm{Fe}_\mathrm{G} \times F_* + \mathrm{offset}_\mathrm{Fe}. \tag{C.1b}$$

Given that $\delta_{\mathrm{Fe,G}} = \delta_{\mathrm{Zn,G}} + [\mathrm{Fe/Zn}]_\mathrm{G}$ (see Fig. 1, regardless of the offsets), then Eq. (C.1a) can be rewritten as

$$\delta_{\mathrm{Fe,G}} - [\mathrm{Fe/Zn}]_\mathrm{G} = d\mathrm{Zn}_\mathrm{G} \times F_*. \tag{C.2}$$

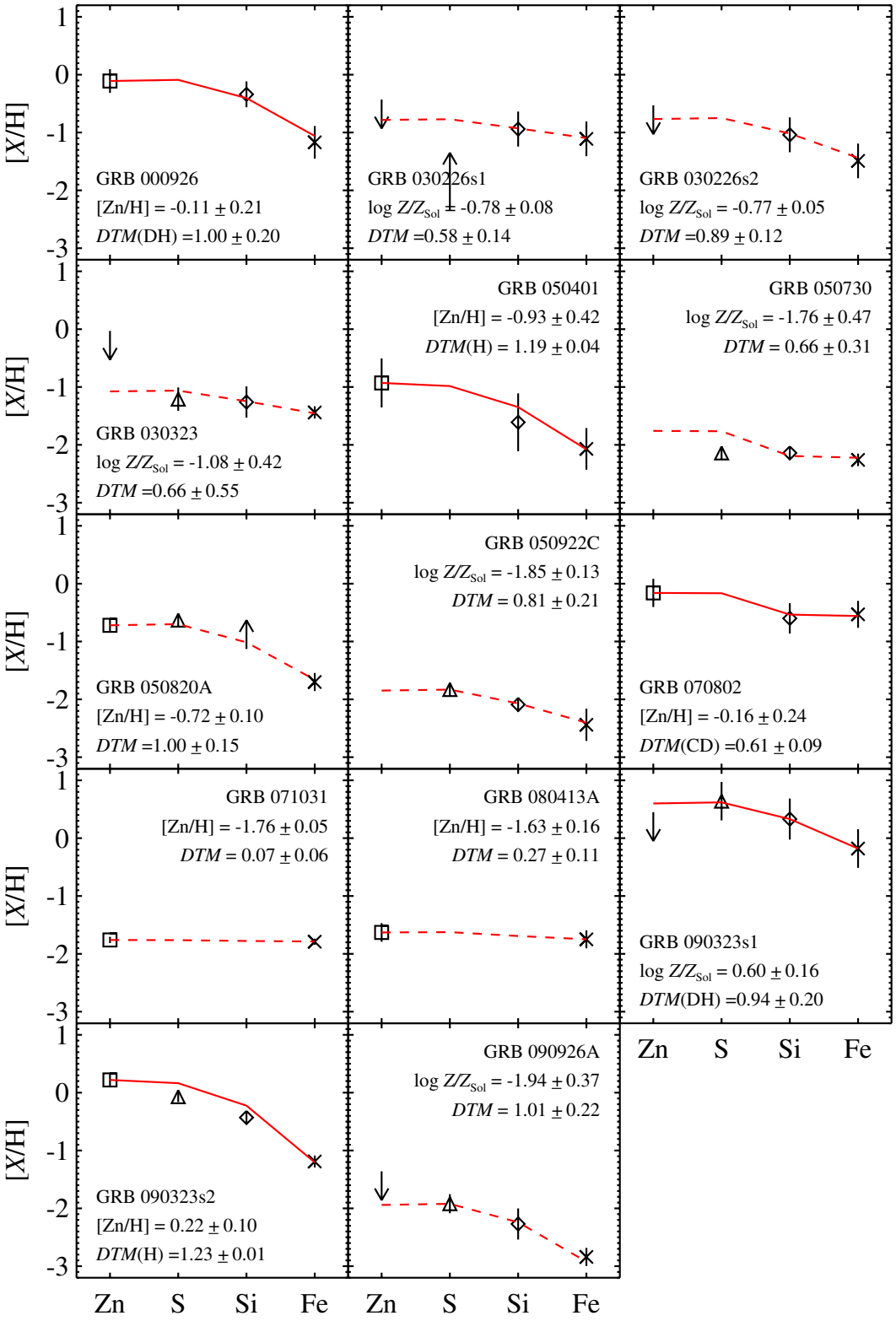

Fig. C.1. Depletion pattern [X/H] observed in GRB absorbers. The solid lines represent the best-fit depletion patterns corresponding to a best-fit dust-to-metal ratio, environment type, and metallicity, labeled on each panel and reported in Table 1. [Zn/H] are used as metallicity input for the fit, while $\log Z/Z_\odot$ are the fitted metallicities in case the H I column density, rather than N(Zn II) is constrained. The dashed lines refer to those cases where a single environment type could not be constrained. All upper and lower limits, as well as any constraint on sulphur are not included in the fit, but only displayed for completeness.

Deriving F_* from Eq. (C.1b) and substituting in Eq. (C.1a) provides

$$\delta_{\mathrm{Fe,G}} - [\mathrm{Fe/Zn}]_\mathrm{G} = \frac{d\mathrm{Zn_G}}{d\mathrm{Fe_G}}\,(\delta_{\mathrm{Fe,G}} - \mathrm{offset_{Fe}}).$$

From dtm = $1 - 10^{\delta_{\mathrm{Fe}}}$ (Eq. (5)) it finally follows that

$$\mathrm{dtm(G)} = 1 - 10^{([\mathrm{Fe/Zn}]_\mathrm{G}\, d\mathrm{Fe_G} - \mathrm{offset_{Fe}}\, d\mathrm{Zn_G})/(d\mathrm{Fe_G} - d\mathrm{Zn_G})} = 0.89. \quad \text{(C.3)}$$

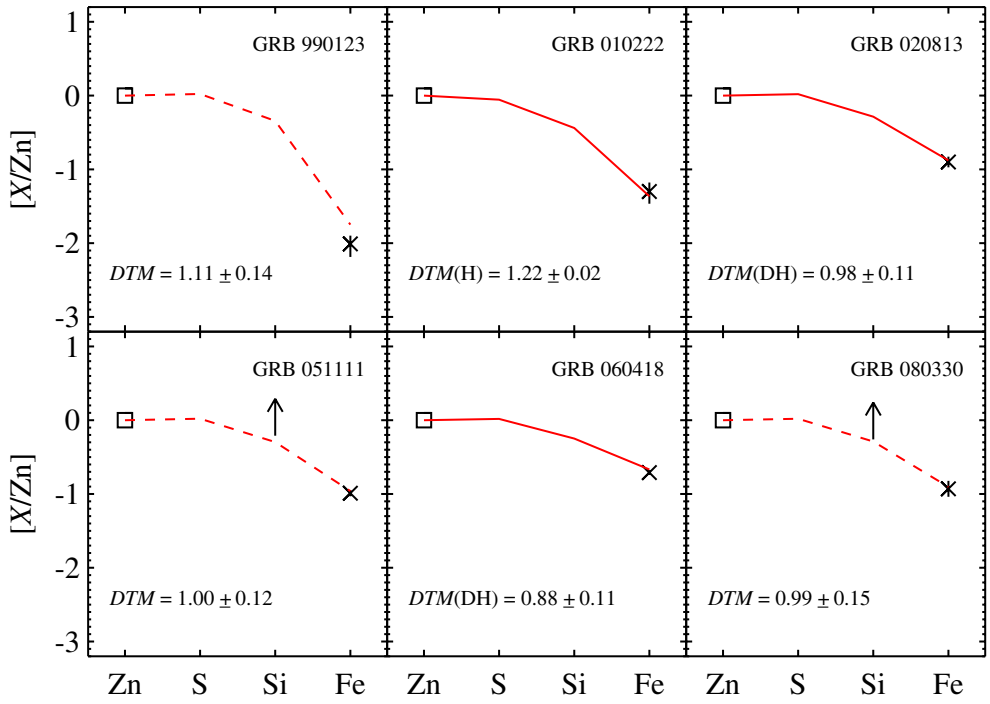

Fig. C.2. Same as Fig. C.1, except for those cases where N(H I) is not constrained, so the relative abundances with respect to Zn, [X/Zn] are fitted instead of the absolute abundances.

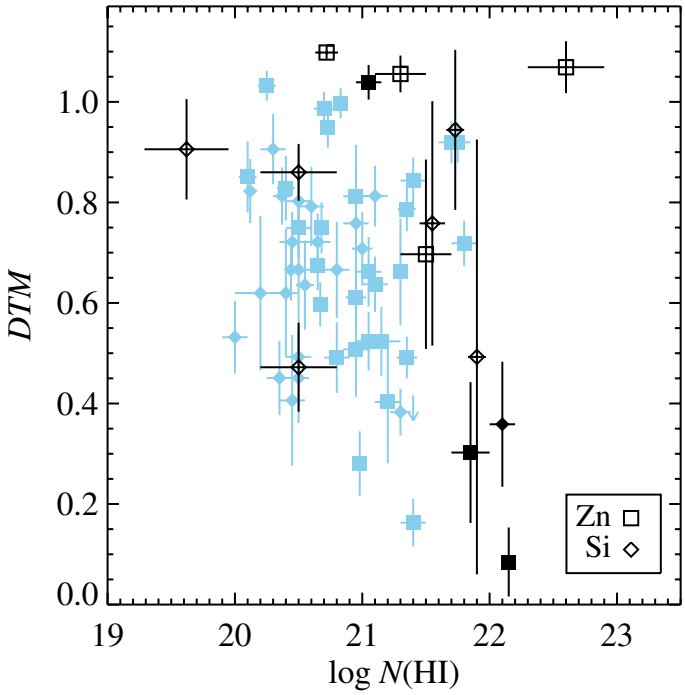

Fig. C.3. $\mathcal{DTM}$ distribution with the H I column density. The symbols are the same as in Fig. 3.

References

Asplund, M., Grevesse, N., Sauval, A. J., & Scott, P. 2009, ARA&A, 47, 481
Berger, E., Penprase, B. E., Cenko, S. B., et al. 2006, ApJ, 642, 979
Bohlin, R. C., Savage, B. D., & Drake, J. F. 1978, ApJ, 224, 132
Brinchmann, J., Charlot, S., Kauffmann, G., et al. 2013, MNRAS, 432, 2112
Campana, S., Romano, P., Covino, S., et al. 2006, A&A, 449, 61
Charlot, S., & Longhetti, M. 2001, MNRAS, 323, 887
Chen, H.-W., Perley, D. A., Pollack, L. K., et al. 2009, ApJ, 691, 152
Cortese, L., Ciesla, L., Boselli, A., et al. 2012, A&A, 540, A52
Dai, X., & Kochanek, C. S. 2009, ApJ, 692, 677
De Cia, A., Ledoux, C., Fox, A. J., et al. 2012, A&A, 545, A64
Dekker, H., D'Odorico, S., Kaufer, A., Delabre, B., & Kotzlowski, H. 2000, in SPIE Conf. Ser. 4008, eds. M. Iye, & A. F. Moorwood, 534
D'Elia, V., Fiore, F., Perna, R., et al. 2009, A&A, 503, 437
Dessauges-Zavadsky, M., Chen, H., Prochaska, J. X., Bloom, J. S., & Barth, A. J. 2006a, ApJ, 648, L89
Dessauges-Zavadsky, M., Prochaska, J. X., D'Odorico, S., Calura, F., & Matteucci, F. 2006b, A&A, 445, 93
Di Criscienzo, M., Dell'Agli, F., Ventura, P., et al. 2013, MNRAS, 433, 313
Draine, B. T. 2003, ARA&A, 41, 241
Draine, B. T., & Hao, L. 2002, ApJ, 569, 780
Draine, B. T., Dale, D. A., Bendo, G., et al. 2007, ApJ, 663, 866
Elíasdóttir, Á., Fynbo, J. P. U., Hjorth, J., et al. 2009, ApJ, 697, 1725
Evans, P. A., Beardmore, A. P., Page, K. L., et al. 2009, MNRAS, 397, 1177
Field, G. B. 1974, ApJ, 187, 453
Fynbo, J. P. U., Jakobsson, P., Prochaska, J. X., et al. 2009, ApJS, 185, 526
Galama, T. J., & Wijers, R. A. M. J. 2001, ApJ, 549, L209
Gall, C., Andersen, A. C., & Hjorth, J. 2011a, A&A, 528, A13
Gall, C., Andersen, A. C., & Hjorth, J. 2011b, A&A, 528, A14
Gall, C., Hjorth, J., & Andersen, A. C. 2011c, A&ARv, 19, 43
Galliano, F., Dwek, E., & Chanial, P. 2008, ApJ, 672, 214
Güver, T., & Özel, F. 2009, MNRAS, 400, 2050
Herrera-Camus, R., Fisher, D. B., Bolatto, A. D., et al. 2012, ApJ, 752, 112
Hirashita, H., & Kuo, T.-M. 2011, MNRAS, 416, 1340
Hjorth, J., & Bloom, J. S. 2012, in The Gamma-Ray Burst – Supernova Connection, (Cambridge: Cambridge University Press), 169
Hjorth, J., Vreeswijk, P. M., Gall, C., & Watson, D. 2013, ApJ, 768, 173
Hunt, L., Palazzi, E., Rossi, A., et al. 2011, ApJ, 736, L36
Jenkins, E. B. 2009, ApJ, 700, 1299
Karakas, A., & Lattanzio, J. C. 2007, PASA, 24, 103
Khare, P., vanden Berk, D., York, D. G., Lundgren, B., & Kulkarni, V. P. 2012, MNRAS, 419, 1028
Kimura, H., Mann, I., & Jessberger, E. K. 2003, ApJ, 583, 314
Krühler, T., Greiner, J., Schady, P., et al. 2011, A&A, 534, A108
Krühler, T., Ledoux, C., Fynbo, J. P. U., et al. 2013, A&A, 557, A18
Kuo, T.-M., & Hirashita, H. 2012, MNRAS, 424, L34
Ledoux, C., Bergeron, J., & Petitjean, P. 2002, A&A, 385, 802
Ledoux, C., Petitjean, P., & Srianand, R. 2006, ApJ, 640, L25
Ledoux, C., Vreeswijk, P. M., Smette, A., et al. 2009, A&A, 506, 661
Lodders, K., Palme, H., & Gail, H.-P. 2009, in Landolt-Börnstein – Group VI Astronomy and Astrophysics Numerical Data, ed. J. E. Trümper, 44

Martin, N., Maurice, E., & Lequeux, J. 1989, A&A, 215, 219
Matsuura, M., Dwek, E., Meixner, M., et al. 2011, Science, 333, 1258
Mattsson, L. 2011, MNRAS, 414, 781
Mattsson, L., Andersen, A. C., & Munkhammar, J. D. 2012, MNRAS, 423, 26
Ménard, B., Nestor, D., Turnshek, D., et al. 2008, MNRAS, 385, 1053
Molaro, P., Bonifacio, P., Centurión, M., et al. 2000, ApJ, 541, 54
Morgan, H. L., & Edmunds, M. G. 2003, MNRAS, 343, 427
Morrison, R., & McCammon, D. 1983, ApJ, 270, 119
Noterdaeme, P., Ledoux, C., Petitjean, P., & Srianand, R. 2008, A&A, 481, 327
Pei, Y. C. 1992, ApJ, 395, 130
Perley, D. A., Levan, A. J., Tanvir, N. R., et al. 2013, ApJ, submitted [arXiv:1301.5903]
Pinto, C., Kaastra, J. S., Costantini, E., & de Vries, C. 2013, A&A, 551, A25
Piran, T. 1999, Phys. Rep., 314, 575
Pirronello, V., Biham, O., Liu, C., Shen, L., & Vidali, G. 1997, ApJ, 483, L131
Predehl, P., & Schmitt, J. H. M. M. 1995, A&A, 293, 889
Prochaska, J. X., Chen, H., Dessauges-Zavadsky, M., & Bloom, J. S. 2007, ApJ, 666, 267
Prochaska, J. X., Sheffer, Y., Perley, D. A., et al. 2009, ApJ, 691, L27
Przybilla, N., Nieva, M.-F., & Butler, K. 2008, ApJ, 688, L103
Rossi, A., Klose, S., Ferrero, P., et al. 2012, A&A, 545, A77
Roth, K. C., & Blades, J. C. 1995, ApJ, 445, L95
Sandstrom, K. M., Bolatto, A. D., Bot, C., et al. 2012, ApJ, 744, 20
Sari, R., Piran, T., & Narayan, R. 1998, ApJ, 497, L17
Savage, B. D., & Sembach, K. R. 1996, ARA&A, 34, 279
Savaglio, S. 2001, in The Extragalactic Infrared Background and its Cosmological Implications, eds. M. Harwit, & M. G. Hauser, IAU Symp., 204, 307
Savaglio, S., & Fall, S. M. 2004, ApJ, 614, 293
Savaglio, S., Fall, S. M., & Fiore, F. 2003, ApJ, 585, 638
Savaglio, S., Glazebrook, K., & Le Borgne, D. 2009, ApJ, 691, 182
Savaglio, S., Rau, A., Greiner, J., et al. 2012, MNRAS, 420, 627
Schady, P., Page, M. J., Oates, S. R., et al. 2010, MNRAS, 401, 2773
Schady, P., Savaglio, S., Krühler, T., Greiner, J., & Rau, A. 2011, A&A, 525, A113
Schady, P., Dwelly, T., Page, M. J., et al. 2012, A&A, 537, A15
Sofia, U. J., Gordon, K. D., Clayton, G. C., et al. 2006, ApJ, 636, 753
Tielens, A. G. G. M., McKee, C. F., Seab, C. G., & Hollenbach, D. J. 1994, ApJ, 431, 321
Valiante, R., Schneider, R., Salvadori, S., & Bianchi, S. 2011, MNRAS, 416, 1916
Ventura, P., Criscienzo, M. D., Schneider, R., et al. 2012, MNRAS, 424, 2345
Vergani, S. D., Petitjean, P., Ledoux, C., et al. 2009, A&A, 503, 771
Vladilo, G. 1998, ApJ, 493, 583
Vladilo, G. 2004, A&A, 421, 479
Voshchinnikov, N. V., & Henning, T. 2010, A&A, 517, A45
Vreeswijk, P. M., Ellison, S. L., Ledoux, C., et al. 2004, A&A, 419, 927
Vreeswijk, P. M., Ledoux, C., Smette, A., et al. 2007, A&A, 468, 83
Vreeswijk, P. M., Ledoux, C., Smette, A., et al. 2011, A&A, 532, C3
Vreeswijk, P. M., Ledoux, C., Raassen, A. J. J., et al. 2013, A&A, 549, A22
Watson, D. 2011, A&A, 533, A16
Waxman, E., & Draine, B. T. 2000, ApJ, 537, 796
Welty, D. E., Lauroesch, J. T., Blades, J. C., Hobbs, L. M., & York, D. G. 1997, ApJ, 489, 672
Welty, D. E., Frisch, P. C., Sonneborn, G., & York, D. G. 1999, ApJ, 512, 636
Welty, D. E., Lauroesch, J. T., Blades, J. C., Hobbs, L. M., & York, D. G. 2001, ApJ, 554, L75
Wilms, J., Allen, A., & McCray, R. 2000, ApJ, 542, 914
Wolfe, A. M., Turnshek, D. A., Smith, H. E., & Cohen, R. D. 1986, ApJS, 61, 249
Wolfe, A. M., Gawiser, E., & Prochaska, J. X. 2005, ARA&A, 43, 861
Woosley, S. E. 1993, ApJ, 405, 273
Zafar, T., & Watson, D. 2013, A&A, 560, A26
Zafar, T., Watson, D., Fynbo, J. P. U., et al. 2011a, A&A, 532, A143
Zafar, T., Watson, D. J., Tanvir, N. R., et al. 2011b, ApJ, 735, 2
Zafar, T., Watson, D., Elíasdóttir, Á., et al. 2012, ApJ, 753, 82